Mu-Zero Resonance Antenna

Jae-Hyun Park, Young-Ho Ryu, and Jeong-Hae Lee, *Member, IEEE*

***Abstract*—We present mu-zero resonance (MZR) antennas that use an artificial mu-negative (MNG) transmission line (TL). The equivalent circuit for verifying the peculiarity of the MNG TL is derived and analyzed. To operate the MZR antenna properly, the antenna is fed by magnetic coupling. The analysis and design of the MZR antenna are performed according to theory and simulation based on a dispersion diagram and field distribution. The surface current distribution shows that the radiation mechanism of the MZR antenna is essentially identical to that of a small-loop antenna. Applying the novel concept of the MZR antenna, a dual-band MZR antenna using two MZR antennas with different MZR frequencies is proposed. The radiation characteristics of the antenna are simulated and measured at two frequencies. The measured characteristics show agreement with the simulated results. It is confirmed that the characteristics of the MZR antenna, including the efficiency, gain, and fractional bandwidth, are suitable for a multiband antenna.**

***Index Terms*—Metamaterials, mu-negative (MNG), mu-zero resonance (MZR), small-loop antenna.**

I. Introduction

THE novel electromagnetic properties of metamaterials [1]–[5], such as backward-wave propagation, the negative index refraction, and the infinite wavelength wave have opened up new areas of applications. Since the beginning of research on this area, the field and the number of applications of metamaterials have shown rapid growth. From a practical application standpoint, the composite right- and left-handed (CRLH) transmission line (TL) has been broadly applied to radio frequency (RF) devices because it is associated with a low level of loss and a broad LH bandwidth [6]–[9]. In addition, the CRLH TL provides an inherent parasitic right-handed property because it contains the same components utilized in a conventional TL. Therefore, the CRLH TL has the unique property of an infinite wavelength wave (zero propagation constant) at a discrete frequency of the boundary of the LH and RH bands. Various size-independent RF devices using the infinite wavelength property of the CRLH TL, such as a power divider [10], a zeroth-order resonator (ZOR) [11], and ZOR antennas [12]–[19] have been reported.

Recently, a ZOR antenna based on the fundamental infinite wavelength property of a shunt inductor-loaded TL [18] or an artificial epsilon-negative (ENG) TL [19] was presented. Given that an infinite wavelength occurs at the zero permittivity of the metamaterial TL, the epsilon-zero resonance (EZR) frequency does not depend on its electrical length, which is similar to the ZOR frequency of the CRLH TL [11]–[16]. The CRLH TL has two ZOR resonances which depend on the applied boundary condition because the TL consists of a combination of series and shunt resonances. To realize ZOR antennas using the ZORs of CRLH and ENG TLs in a number of studies [11]–[19], an open-ended boundary condition was applied because the antennas are implemented by the shunt admittance of a unit cell, which determines the ZOR frequency where the effective permittivity is zero.

In this paper, a mu-zero resonance (MZR) antenna which also supports an infinite wavelength wave is proposed using an artificial mu-negative (MNG) TL [see Fig. 1]. The TL has an effectively negative mu value in the rejection band due to its artificially added series capacitance, which is similar to the ENG TL [18], [19]. Therefore, the artificial MNG TL provides a MNG rejection band in the low-frequency region and a right-handed (RH) propagation band in the high-frequency region [see Fig. 2]. Therefore, at the transition point between the MNG rejection and RH propagation bands, the MNG TL has the MZR mode of zero permeability. By varying the series capacitance of the MNG TL unit cell, the MZR frequency of the resonator using the MNG TL can be controlled. To design the MZR antenna, a short-ended boundary condition must be applied to the antenna because the series resonance of the MNG TL unit cell determines the MZR frequency, which supports the infinite wavelength, while an open-boundary condition is applied to the antenna using CRLH and ENG TLs. A matching network using a magnetic coupling to operate the MZR antenna effectively is numerically verified. MZR antennas consisting of one, two, and three unit cells are investigated based on periodic structure theory, circuit modeling with an optimized parameter, full-wave simulation, and measurements. It is shown that the MZR antenna has good efficiency, gain, and fractional bandwidth characteristics. Furthermore, MZR antennas are suitable for multiband applications because they can be coupled and integrated by one feed line. A dual-band antenna using two mu-zero resonators as an example is presented.

II. Theory

The artificial MNG TL supporting an infinite wavelength is discussed in Section II-A. The resonator using the TL is also analyzed in Section II-B.

Manuscript received June 19, 2008; revised January 24, 2009; accepted January 01, 2010. Date of publication March 29, 2010; date of current version June 03, 2010. This work was supported by the Korea Science and Engineering Foundation (KOSEF) grant funded by the Korean government (MOST) (No. R01-2007-000-20495-0) .

J.-H. Park is with the Department of Electronic Information and Communication Engineering, Hongik University, Seoul 121-791, Korea.

Y.-H. Ryu is with the School of Electrical Engineering and Computer Science, Kyungpook National University, Daegu 702-701, Korea.

J.-H. Lee is with the Department of Electronic and Electrical Engineering, Hongik University, Seoul 121-791, Korea (e-mail: jeonglee@hongik.ac.kr).

Color versions of one or more of the figures in this paper are available online at http://ieeexplore.ieee.org.

Digital Object Identifier 10.1109/TAP.2010.2046832

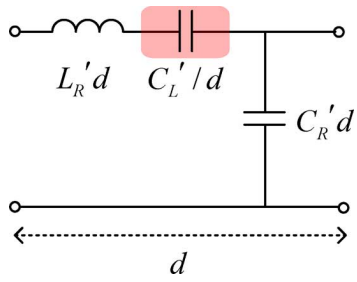

Fig. 1. Equivalent circuit of a lossless artificial MNG TL.

A. Infinite Wavelength Property of Artificial Mu-Negative Transmission Line

In general, practically realized metamaterial TLs are composed of artificial components such as via holes, gaps, stubs and other such components. Thus, the equivalent circuit of a lossless ($R = 0$ and $G = 0$) artificial mu-negative (MNG) TL is realized by adding a series capacitance (C_L') to the host TL, as shown in Fig. 1. The effective permeability and permittivity of the MNG TL are then obtained through the equation below, which is similar to CRLH and ENG TLs [19]

$$\mu = \frac{Z'}{j\omega} = L_R' - \frac{1}{\omega^2 C_L'}$$
$$\varepsilon = \frac{Y'}{j\omega} = C_R'. \tag{1}$$

Here, C_L', C_R', and L_R' are the times-unit-length series capacitance, the per-unit-length shunt capacitance, and the per-unit-length series inductance in terms of an infinitesimal component (in $\mathrm{F}\cdot\mathrm{m}$, *F/m*, and *H/m*), respectively.

The propagation constant of the MNG TL can be obtained by applying periodic boundary conditions to the equivalent circuit of the unit cell, as follows [4]

$$\beta d = \cos^{-1}\left\{1 - \frac{1}{2}\left(\frac{\omega^2 - {\omega_M}^2}{{\omega_R}^2}\right)\right\} \tag{2}$$

where

$$\omega_R = \frac{1}{\sqrt{L_R C_R}} \text{ and } \omega_M = \frac{1}{\sqrt{L_R C_L}} \tag{3}$$

β is the propagation constant for Bloch waves, and d is length of the unit cell. C_L ($= C_L'/d$), C_R ($= C_R'd$), and L_R ($= L_R'd$) are the series capacitance, shunt capacitance, and series inductance in terms of the real lumped component (in *F* and *H*), respectively.

From (2), the dispersion curve of the MNG TL is obtained and those of the CRLH and ENG TLs are over plotted to compare with the ZOR frequencies of each TL, as shown in Fig. 2. The equivalent circuit elements used in plotting the dispersion curves are $C_L = 2$ pF, $C_R = 1$ pF, $L_L = 1$ nH, and $L_R = 1$ nH, respectively, in Fig. 1. (Here, L_L is the shunt inductance for the CRLH and ENG TLs in the literature [18], [19]). In Fig. 2, the corresponding mu-zero (f_M) and epsilon-zero (f_E) frequencies are 3.56 GHz and 5.03 GHz, respectively. An artificial MNG TL, similar to the ENG TL, supports zero and positive propagation constants while the propagation constants of the CRLH TL are negative, zero, and positive values [11]–[15], as shown in Fig. 2. Therefore, the MNG TL also has an infinite wavelength property with a zero propagation constant. Depending on the boundary condition, the ZOR frequencies of each TL are selected. That is, the mu-zero resonance (MZR) is obtained with a short-ended boundary condition while the epsilon-zero resonance (EZR) is obtained with an open-ended boundary condition. Therefore, the MNG TL has a nonzero resonance frequency (f_M), which is supported by the series resonance of the TL unit cell in Fig. 1. In this case, a short-ended boundary must be employed to apply the MZR to RF devices.

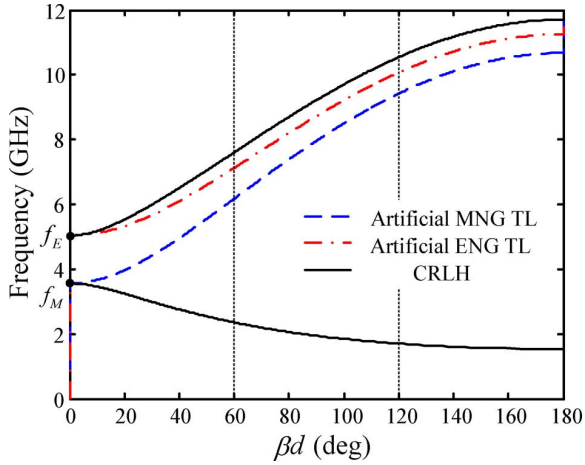

Fig. 2. Dispersion relations of the metamaterial TLs.

B. Resonators Using an Artificial Mu-Negative Transmission Line

The resonance modes of the MNG TL can be obtained by the following simple condition, similar to those of the CRLH and ENG TLs [11]–[19]:

$$\beta_n d = \frac{n\pi d}{l} = \frac{n\pi}{N}, \text{ where } n = 0, 1, 2, \ldots, (N-1) \tag{4}$$

where N ($= l/d$) and l are the number of the unit cell and the total length of the resonator, respectively.

To calculate the theoretical MZR frequency of the MNG TL, the input impedances of conventional TLs based on the open- and short-ended boundary conditions are calculated by (5) [11]

$$\begin{aligned}&\text{Open-ended boundary condition:}\\ &Z_{in} = -jZ_0 \cot \beta d^{\beta\to 0}\\ &\quad = -jZ_0\frac{1}{\beta d} = -j\sqrt{\frac{Z}{Y}}\left(\frac{1}{-j\sqrt{ZY}}\right)\frac{1}{N} = \frac{1}{NY}\\ &\text{Short-ended boundary condition:}\\ &Z_{in} = jZ_0 \tan \beta d^{\beta\to 0}\\ &\quad = jZ_0\beta d = j\sqrt{\frac{Z}{Y}}\left(-j\sqrt{ZY}\right)N = NZ.\end{aligned} \tag{5}$$

By applying the conditions to the equivalent circuit in Fig. 1, (5) can be rewritten as

$$\begin{aligned}&\text{Open-ended boundary condition:}\\ &Z_{in} = \frac{1}{j\omega N C_R}\\ &\text{Short-ended boundary condition:}\\ &Z_{in} = j\omega N L_R + \frac{N}{j\omega C_L}.\end{aligned} \tag{6}$$

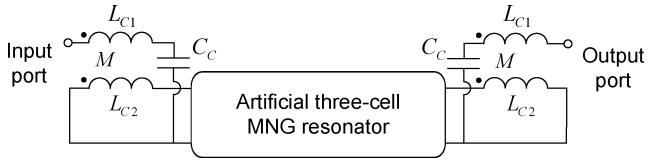

Fig. 3. Schematic diagram for the short-ended resonator using an artificial three-stage MNG TL by magnetic coupling.

To obtain the MZR frequency, the short-ended boundary condition must be applied to the unit cell from (6). Thus, the MZR frequency, similar to those of the CRLH and ENG TLs, is given as

$$\omega_{MZR} = \omega_M = \frac{1}{\sqrt{L_R C_L}}. \tag{7}$$

From (7), it is noted that the resonant frequency is independent of the total length (Nd) of the resonators.

Fig. 3 shows a schematic diagram of the short-ended resonator using an artificial three-stage MNG TL, which is related to the equivalent circuit of Fig. 1. The same circuit parameter values of Fig. 2 are used in the simulation. In Fig. 3, the short-ended resonator is connected to the magnetic coupled section with input and output ports for magnetic coupling in the resonator. The parameter values are arbitrarily chosen to be $C_C = 1$ pF, $L_{C1} = 1$ nH, and $L_{C2} = 0.1$ nH, with mutual inductance of $M = 0.2$ nH between the L_{C1} and L_{C2} in order to achieve a magnetic coupling of the mu-zero resonators to external ports and show that the CRLH and MNG TLs have the same ZOR frequency.

To verify the related resonance modes in (4) and (7), the resonant frequencies of the resonator in Fig. 3 were simulated using a circuit simulator (Ansoft's Designer). Fig. 4 shows the simulation results with that of the CRLH TL case for comparison. The three-stage CRLH resonator has two negative, two positive, and zero resonance modes while the three-stage MNG resonator has two positive and zero resonance modes, as shown in Fig. 4. In particular, the MZR frequency (f_{MZR}) of the MNG resonator is identical to that of the CRLH resonator in spite of absence of the shunt inductance in the short-ended MNG and CRLH resonators, similar to the open-ended ENG and CRLH resonators [18], [19]. Thus, the MNG resonator has a simpler structure and is easier to fabricate than the CRLH resonator, as the shunt components of the CRLH TL, such as metallic vias, are not required.

In Table I, the simulated resonance frequencies of the MNG and CRLH resonators are compared with the theoretical resonance frequencies of the resonators in Fig. 2. It is noted that each βd value of 0°, 60°, and 120° in Fig. 2 corresponds to the resonant modes of the zero, first, and second modes, respectively. The simulated results show good agreement with the theory, as shown in Table I. The slight difference in the resonance frequencies at each mode is caused by the boundary conditions. That is, the theoretical resonant frequencies are obtained with the perfectly short-ended boundary condition, whereas the simulated resonance frequencies are shifted by the coupling coefficients from the C_C, M, L_{C1}, and L_{C2} values at each mode, as shown in Fig. 3. Consequently, the infinite wavelength resonator using the artificial MNG TL with the short-ended boundary condition can be successfully applied to the antennas because the antenna size will be independent of the electrical length and because they are easily fabricated.

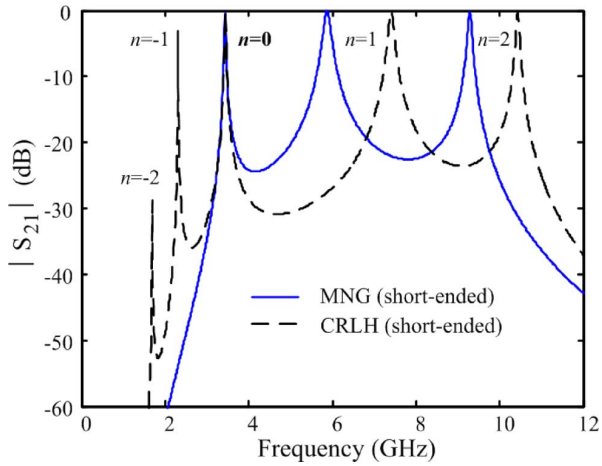

Fig. 4. Resonance modes of the three-stage MNG and CRLH resonators.

TABLE I
RESONANCE MODES OF THREE-CELL MNG AND CRLH RESONATORS

	-2 mode	-1 mode	0 mode	1 mode	2 mode
	Circuit simulation / Theoretical analysis (GHz)				
Three-cell MNG resonator			3.44/ 3.56	5.87 / 6.16	9.28 / 9.42
Three-cell CRLH resonator	1.69 / 1.70	2.31 / 2.36	3.44/ 3.56	7.40 / 7.60	10.43 / 10.54

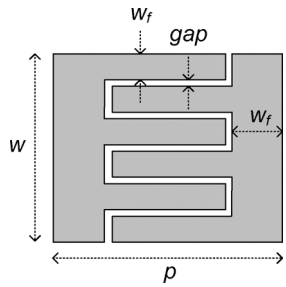

Fig. 5. Unit cell of artificial MNG TL ($\text{gap} = 0.1$ mm, $w_f = 0.15$ mm, and $p = 3$ mm).

III. MU-ZERO RESONANCE ANTENNA

A. Realization of an Artificial MNG TL

To realize the miniaturized artificial MNG TL, an interdigital capacitor (IDC) is employed, as shown in Fig. 5. A unit-cell structure has the following dimensions: gap of 0.1 mm, a finger width (w_f) of 0.15 mm, and a period (p) of 3 mm. The substrate of the MNG TL uses a Rogers RT/Duroid 5880 with a dielectric constant $\varepsilon_r = 2.2$ and a thickness $h = 1.57$ mm. As mentioned in Section II-A, the effective permeability of the MNG TL has negative, zero, and positive values due to the series capacitance of the IDC. The TL has a MZR frequency at zero permeability, which can be controlled by the number of fingers (n_f) of the IDC. Thus, the parameters of a related number of fingers were studied using a circuit and full-wave simulator.

TABLE II
EXTRACTED PARAMETERS OF MNG UNIT CELL VERSUS NUMBER OF FINGERS

Number of fingers (n_f)	Extracted parameters (unit cell simulation)			
	C_L (pF)	L_R (nH)	C_R (pF)	f_{MZR} (GHz)
4 (w=0.9mm)	0.19	1.94	0.12	8.4
6 (w=1.4mm)	0.29	1.64	0.15	7.3
8 (w=1.9mm)	0.40	1.40	0.17	6.7
10 (w=2.4mm)	0.53	1.19	0.19	6.3

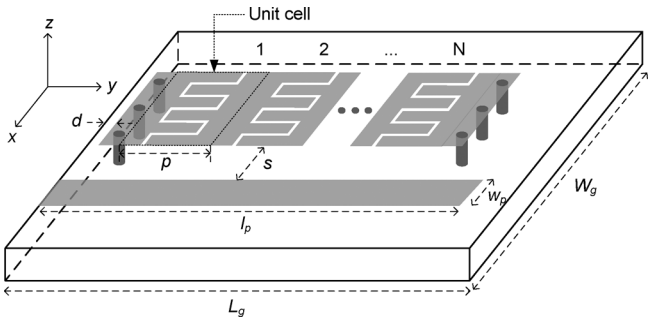

Fig. 6. Mu-zero resonance antenna.

Table II lists the circuit parameters of Fig. 1, as extracted by a full-wave simulation (Ansoft's HFSS) of a MNG unit cell versus the number of fingers. Increasing the number of fingers results in increases in the series capacitance (C_L), as expected, whereas the series inductance (L_R) decreases. Consequently, the MZR frequency decreases because the increment rate of the series capacitance value is larger than the decrement rate of the series inductance value. Thus, to obtain a lower MZR frequency, the number of fingers or length of the unit cell must increase.

B. Antenna Design

Fig. 6 shows the proposed MZR antenna using the MNG resonator with a short-ended boundary. Thus, both ends of the proposed antenna are connected to the ground by metallic via holes. The unit-cell dimensions of the antenna are identical to those discussed in Section III-A. As shown in Fig. 6, the antenna should be located in parallel with the feed line to enhance the magnetic coupling. The antenna uses an open-ended quarter wavelength feed line at the MZR frequency to obtain good impedance matching. The input impedance of the antenna consists of the input impedance of the quarter wavelength feed line and the coupling impedance to the MNG TL.

To investigate the effect of the length of the feed line, the input impedance of the antenna is calculated for three different lengths of feed line: $\lambda/6$ ($l_{\rm p} = 5.3$ mm), $\lambda/4$ ($l_{\rm p} = 7.9$ mm), and $\lambda/3$ ($l_{\rm p} = 10.5$ mm). The length of the feed line has little effect on the MZR frequency, as shown in Fig. 7, because the frequency is mainly determined by the geometrical parameters of the resonator, such as the finger width (w_f), the number of fingers, gap, and the period (p) shown in Fig. 5.

In general, a reactance value must be zero for good impedance matching. However, the imaginary value is not zero when the

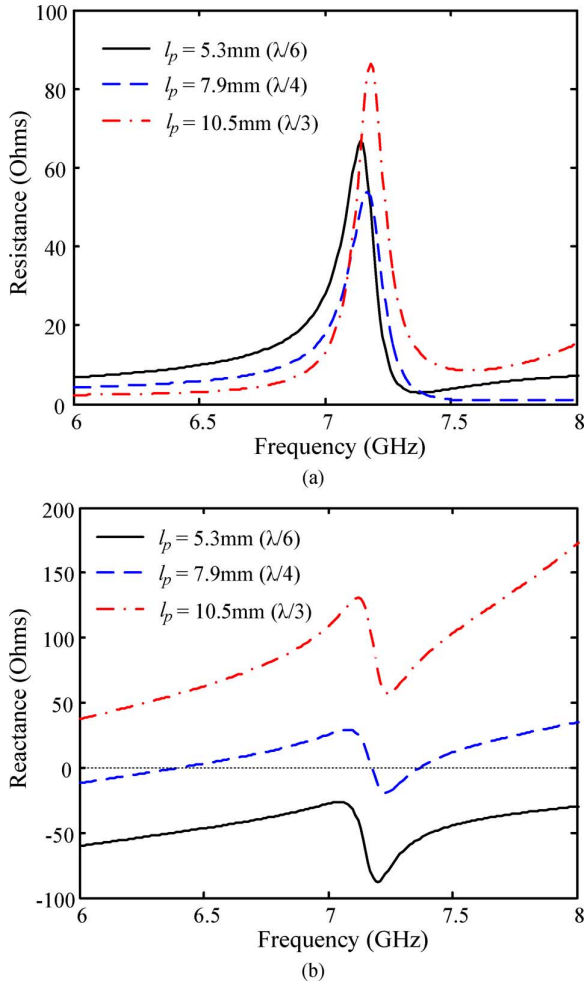

Fig. 7. Input impedance for three different cases (s = 2.5 mm) (a) real and (b) imaginary.

length of the feed line is not a quarter of the wavelength, as shown in Fig. 7(b). Therefore, a rather complex and difficult impedance-matching technique is required if the length of the feed line is not a quarter of the wavelength. Thus, good impedance matching can easily be accomplished using an open-ended quarter-wavelength feed line, as its reactance value at the MZR frequency is zero, as shown in Fig. 7(b).

To investigate the behavior of the input impedance versus the separation (s), a one-cell MZR antenna with an IDC of four fingers was designed and simulated. Fig. 8 shows the input impedance of the port versus the frequency with different separations. The input impedance for matching the antenna can be controlled by the separation between the antenna and the feeding line, which is related to the intensity of the magnetic coupling. That is, if the separation increases, the input impedance decreases due to weak magnetic coupling, as shown in Fig. 8. For instance, an input impedance of $\sim$ 50 Ω is obtained at a separation (s) of 2.5 mm and frequency of 7.16 GHz, as shown in Fig. 8. Consequently, an optimized matching network can be determined according to the separation.

Finally, the width of the feed line is also related to the coupling and impedance matching. If the width is narrower, magnetic coupling is stronger because the narrow feed line has a

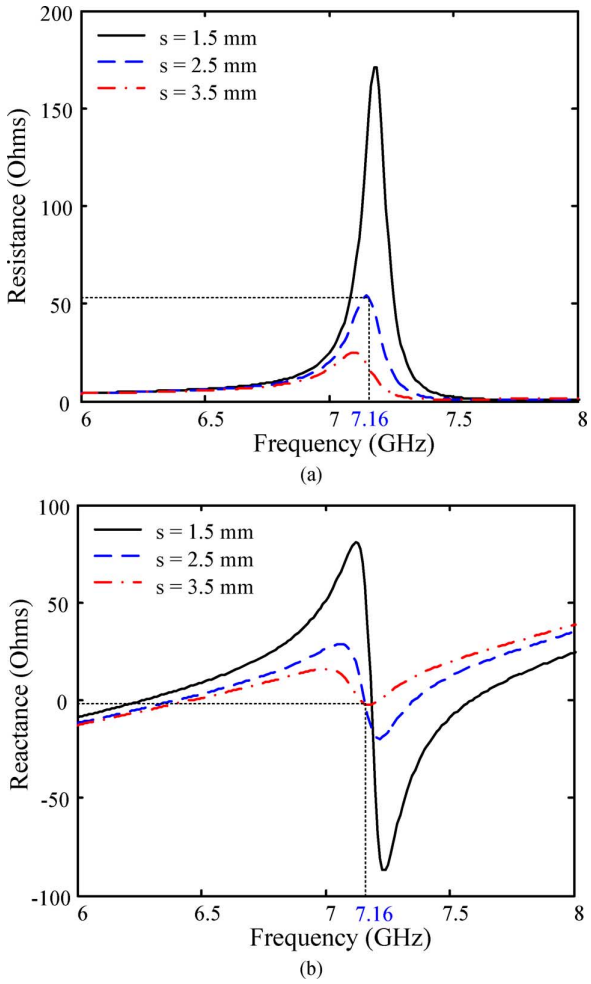

Fig. 8. Input impedance (a) real and (b) imaginary ($w_{\rm p} = 1$ mm, $l_{\rm p} = 7.9$ mm, and $d = 0.55$ mm).

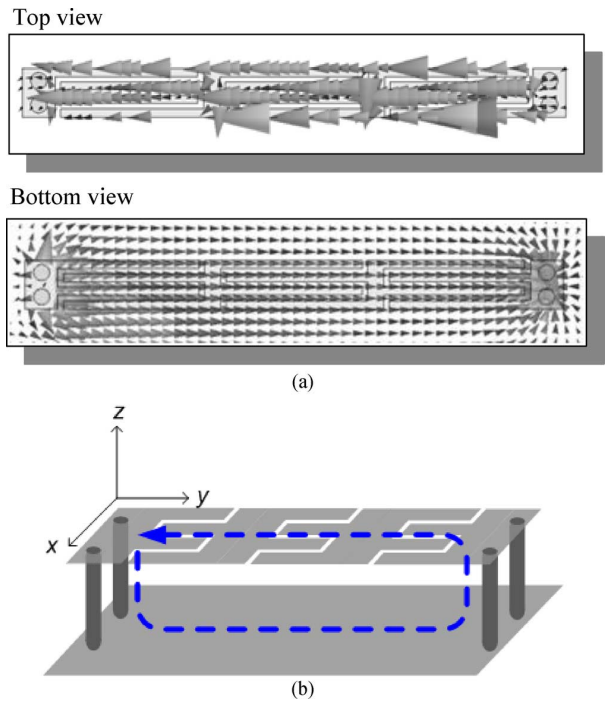

Fig. 9. (a) Simulated surface current of a three-cell MZR antenna at the MZR frequency and (b) equivalent-loop current.

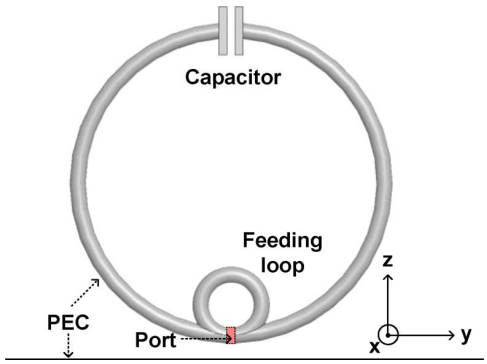

Fig. 10. Simulated small-loop antenna on the ground plane.

strong inductive component. In this study, the width of the antenna was selected as 1 mm to consider the fabrication. If the width of feed line is narrower than 1 mm, the separation (s) must be larger than 2.5 mm.

C. Radiation Mechanism of MZR Antenna

To predict the radiation pattern of the MZR antenna intuitively, the surface current of a three-cell MZR antenna with an IDC of four fingers at the MZR frequency was simulated by Ansoft's HFSS. The surface current flows in opposite directions at the top and bottom in Fig. 9(a), resulting in the equivalent-loop current shown in Fig. 9(b). The surface current intensity is asymmetrical with respect to the y-axis due to the asymmetrical IDC structure and asymmetrical feed structure. Under these circumstances, it is intuitively expected that the radiation patterns of the antenna can be tilted. It is important to note that the phase of the current was observed to be in-phase along the current loop. This indicates that an infinite wavelength is supported at the MZR frequency. As shown in Fig. 9(b), the current flow is identical to that of a small-loop antenna [20]. Therefore, it is expected that the radiation mechanism of the MZR antennas is identical to that of a small-loop antenna. To verify that the MZR antenna has the same radiation properties as a small-loop antenna, the radiation properties of two antennas are simulated and compared in terms of their radiation patterns.

Fig. 10 shows a small-loop antenna above the ground plane. It is oriented vertically with respect to the given coordinate, and a 50 Ω lumped port is applied to the feed. Fig. 11 shows the simulated radiation patterns of a one-cell MZR antenna with an IDC of four fingers and a small-loop antenna above the ground plane. The size and resonance frequency of the two antennas are similar, specifically, $0.09\lambda_0 \times 0.04\lambda_0$ (the length and height of MZR antenna) at 7.16 GHz, and $0.09\lambda_0$ (the diameter of small-loop antenna) at 7.35 GHz, respectively. A parallel plate capacitor was included in a small-loop antenna to reduce its size. The radiation patterns of the two antennas are similar, as expected. A slightly asymmetrical radiation pattern in the MZR antenna was observed due to the asymmetrical IDC structure and asymmetrical feed structure in the x-z plane ($\phi = 0°$). Additionally, a slightly asymmetrical radiation pattern in the MZR antenna on the y-z plane ($\phi = 90°$) occurs because the resonator is placed

TABLE III
EXPERIMENTAL, SIMULATED, AND THEORETICAL RESULTS OF EACH MZR ANTENNA

	f_{MZR} (GHz) exp. / sim. / eqn. (7) / eqn. (9)	Antenna size (W×L)	$\|S_{11}\|$ (dB) exp. / sim.	-10 dB Fractional BW (%) exp. / sim.	Maximum gain (dBi) exp. / sim.	Efficiency (%) exp. / sim.
One-cell ($n_f = 6$)	6.25 / 6.23 / 7.3 / 6.38	5.2 mm×9 mm $0.108\lambda_0 \times 0.188\lambda_0$	-15.2 / -23.5	1.2 / 1.4	1.8 / 3.6	76 / 85
Two-cell ($n_f = 4$)	6.60 / 6.74 / 8.4 / 7.03	4.55 mm×7.9 mm $0.100\lambda_0 \times 0.174\lambda_0$	-15.7 / -28.0	1.4 / 2.1	2.3 / 3.9	80 / 90
Three-cell ($n_f = 4$)	7.30 / 7.32/ 8.4 / 7.58	4.25 mm×7.45 mm $0.103\lambda_0 \times 0.181\lambda_0$	-14.2 / -35.6	2.8 / 4.0	2.9 / 4.7	86 / 95
Four-cell ($n_f = 4$)	7.46 / 7.46 / 8.4 / 7.80	3.50 mm×10.45 mm $0.087\lambda_0 \times 0.260\lambda_0$	-13.5 / -36.0	3.8 / 4.9	3.9 / 5.1	87 / 95

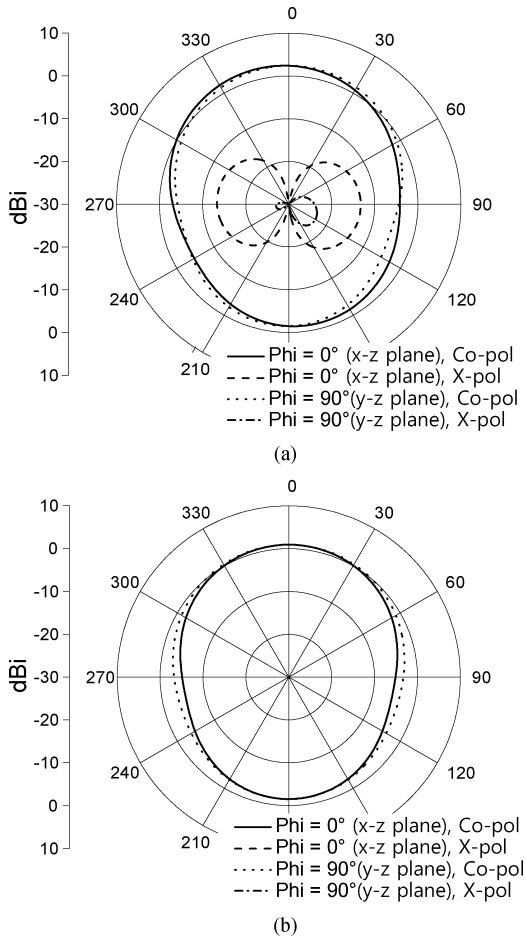

Fig. 11. Simulated radiation patterns (a) One-cell MZR antenna with IDC of four fingers and (b) small-loop antenna ($\mathrm{radius\ of\ loop} = 1.8\ \mathrm{mm}$).

at one side of the feed line. The cross-polarization of the MZR antenna is higher than that of the small loop antenna due to the asymmetric structure, as shown in Fig. 11. Therefore, the MZR antenna as a planar type can be fabricated and integrated with other RF devices more easily compared to a conventional loop antenna that is not a planar type, as shown in Fig. 10. The proposed MZR antenna is also very useful as a multiband antenna.

D. Experimental Results of MZR Antenna

Four types of MZR antennas with the unit cells analyzed in Section III-A were fabricated: Using the unit cells listed in Table II, MZR antennas of a one-cell MZR antenna using an IDC with four fingers, a one-cell MZR antenna using an IDC with six fingers, a two-cell MZR antenna using an IDC with four fingers, and a three-cell MZR antenna with IDC of four fingers were realized. The simulated and measured MZR frequencies, antenna sizes, S_{11} reflection coefficient values, $-10\ \mathrm{dB}$ fractional bandwidths, maximum gains, and radiation efficiencies of the four types of MZR antennas are summarized in Table III. The SMA connector is included in the simulation because the simulated results are compared with those of the measurements.

First, the MZR frequency decreases as the number of fingers increases because the series capacitance increases with the number of fingers. The simulated and measured MZR frequencies converge to the theoretical MZR frequency as the number of unit cells increases because the effect of the metallic vias is removed. It can also be observed that the simulated and measured MZR frequencies are lower than the theoretically calculated frequencies. If inevitable, the inductance (L_{short}) value of the metallic vias for a short-ended boundary is included in an N-stage resonator, as shown in Fig. 6, and the exact input impedance of (6) is modified as

$$Z_{in} = j\omega(NL_R + 2L_{short}) + \frac{N}{j\omega C_L}. \tag{8}$$

Thus, the exact MZR frequency can be obtained by (8), as follows:

$$\omega_{MZR} = \sqrt{\frac{N}{(NL_RC_L + 2L_{short}C_L)}}. \tag{9}$$

If the number of unit cells is infinite ($N = \infty$), the above equation is identical to (7), while if the number of the unit cells decreases, the MZR frequencies from (9) are lower than the theoretical MZR frequency from (7). In Table III, the MZR frequencies that are obtained from (7) and (9) are compared. In (9), the extracted inductance value (L_{short}) of two metallic vias is 0.38 nH. The exact MZR frequency from (9) is closer to the measured and simulated MZR frequencies than that from (7), as shown in Table III. The small difference between the MZR frequency from (9) and the measured and simulated MZR frequencies stems from the coupling effects, as noted in Section II-B. The measured and simulated MZR frequencies are in good agreement, as shown in Table III.

TABLE IV
FINGERS SIMULATED RESULTS OF THE THREE-CELL MZR ANTENNAS WITH THE DIFFERENT GROUND SIZES

Ground size ($W_g \times L_g$)	Frequency (GHz)	Fractional BW (%)	Efficiency (%)	Gain (dBi)
10 mm × 11 mm	7.25	2.22	92	3.8
10 mm × 13.5 mm	7.26	3.78	95	4.4
10 mm × 16 mm	7.31	4.76	96	4.7
10 mm × 18.5 mm	7.35	3.20	94	4.8
10 mm × 21 mm	7.38	2.54	92	4.9
20 mm × 11 mm	7.36	1.47	86	4.6
20 mm × 13.5 mm	7.39	2.08	88	5.3
20 mm × 16 mm	7.40	2.10	89	5.5
20 mm × 18.5 mm	7.39	1.87	88	5.5
20 mm × 21 mm	7.42	1.67	87	5.4

Second, the total size of the MZR antenna becomes relatively large compared to that of the mu-zero resonator because the antenna employs a quarter-wavelength feed line to obtain good matching easily. For example, the total sizes of the one-cell and three-cell MZR antennas with four fingers are $0.100\lambda_0 \times 0.174\lambda_0$ and $0.087\lambda_0 \times 0.260\lambda_0$, as shown in Table III, but the resonator sizes of the MZR antennas are $0.020\lambda_0 \times 0.066\lambda_0$ and $0.022\lambda_0 \times 0.224\lambda_0$, respectively. Thus, smaller MZR antennas can be designed if the quarter-wavelength feed line is replaced by a small matching network. If a small matching network is used, this will affect the value of the input impedance, as shown in Fig. 7, because the magnetic coupling will be affected by the shorter line. Therefore, this has to be considered when designing the matching network.

The important effects of the ground and SMA connector, which affect the properties of the antenna, are also considered. To investigate the effect of the SMA connector, three-cell MZR antennas with and without the SMA connector were simulated. The simulated MZR frequencies and -10 dB fractional bandwidths are 7.46 GHz and 7.40 GHz and 4.9% and 2.1%, respectively. Although the MZR frequencies show good agreement, the bandwidth is rather different because the SMA connector operates as another radiator.

To investigate the ground effect, the antenna properties with respect to the width and length of the ground were simulated using the three-cell MZR antenna without a SMA connector, as shown in Table IV. The simulated results are summarized in Table IV. In general, the size of the ground influences the radiation properties of an antenna and, especially, it affects the bandwidth. When the length of the ground is equal to a half wavelength (16 mm), it is discovered that the antenna has good antenna properties because the ground also radiates. For example, the fractional bandwidth and efficiency increase to 4.76% and 96% when the size of the ground is 10 mm × 16 mm. On the other hand, the fractional bandwidth and efficiency decrease to 2.10% and 89% when the size of ground is 20 mm × 16 mm because ground with a width of 20 mm is matches the feed line less than ground with a width of 10 mm at the MZR frequency.

Dimensions for feed line:
w_p = 1mm, d = 0.55mm
l_p = 7.0mm, and s = 1.6mm

(a)

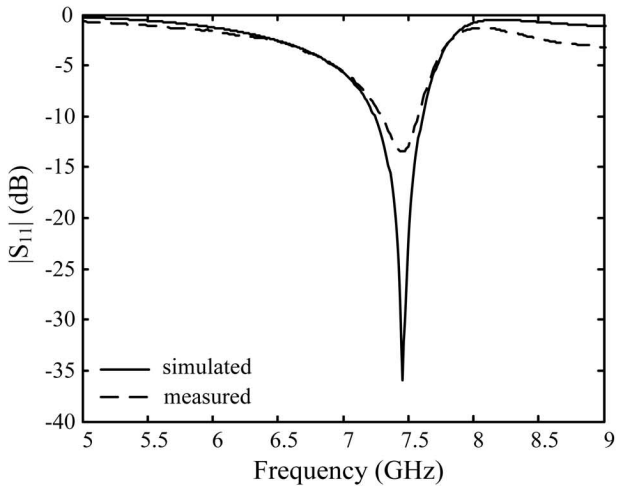

(b)

Fig. 12. Three-cell MZR antenna with IDC of four fingers (a) Photograph, (b) simulated and measured S_{11} reflection coefficient values.

Thus, it cannot be stated that the fractional bandwidth and efficiency decrease with a small ground size. For instance, the fractional bandwidth and efficiency are 2.10% and 89% when the ground size of the fabricated antenna is 20 mm × 16 mm. If it is decreased to 10 mm × 11 mm, the fractional bandwidth and efficiency increase to 2.22% and 92%. In addition, the overall radiation patterns with different ground sizes are similar to that of the small-loop antenna, as shown in Fig. 11. The gain increases as the length of the ground increases in Table IV. The reason for the increment in the gain is that the ground plane is operated as a reflector of radiation. Thus, it is concluded that the fractional bandwidth and efficiency of the MZR antenna are not proportional to the ground size; that is, they can be larger or smaller, as shown in Table IV. Therefore, it is thought that a small MZR antenna with a small ground size of 10 mm × 11 mm listed in Table IV can be designed.

The radiation without the three-cell resonator was calculated to investigate the radiation of the feed line itself and/or the ground. The result shows that the ratio of the radiation power without the MZR resonator to that with the MZR resonator is $\sim 16\%$. However, it was found that some radiated power comes from the ground because the length of the ground (20 mm × 16 mm) in this case was a resonant length of $\lambda/2$. When the length of the ground is changed to 21 mm, which is not $\lambda/2$, the radiated power becomes even smaller ($\sim 12\%$), indicating

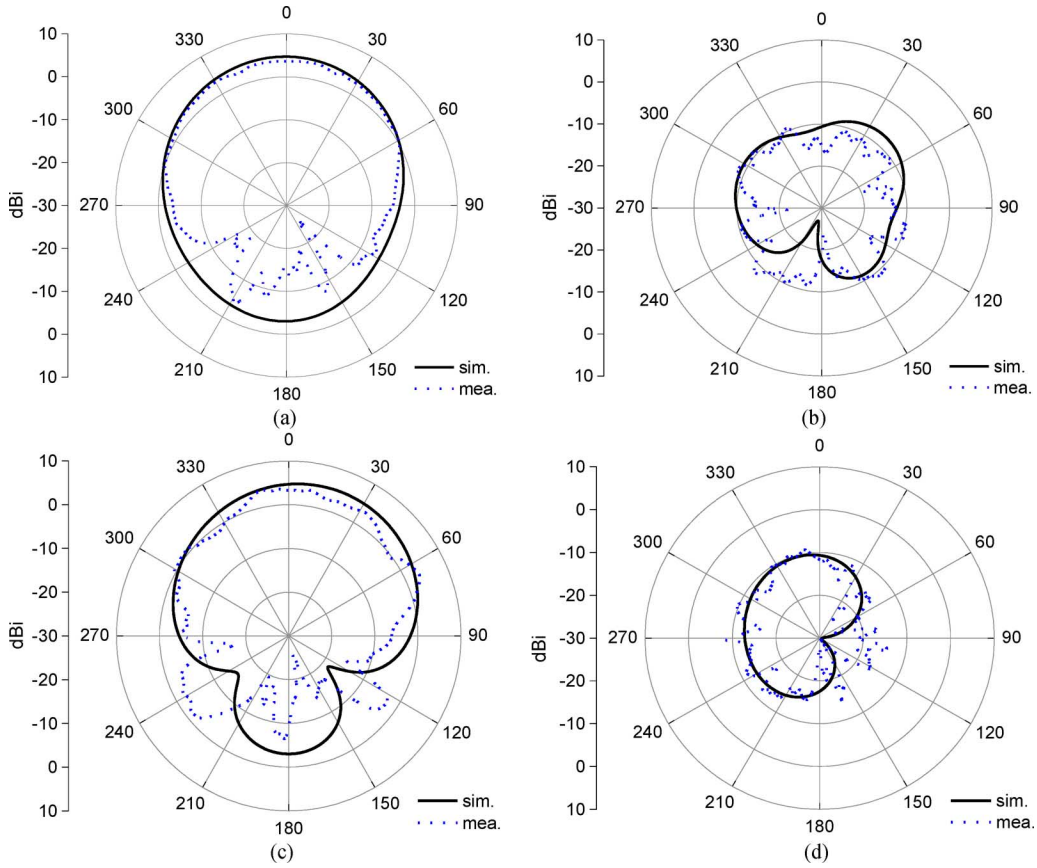

Fig. 13. Radiation patterns of the three-cell MZR antenna ($n_f = 4$): (a) Co-pol. (x-z plane), (b) X-pol. (x-z plane), (c) Co-pol. (y-z plane), (d) X-pol. (y-z plane).

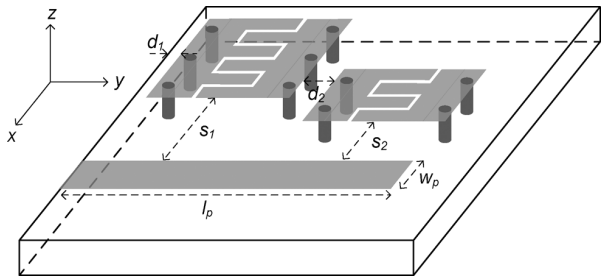

Fig. 14. Dual-band MZR antenna ($n_f = 4$ and $n_f = 6$).

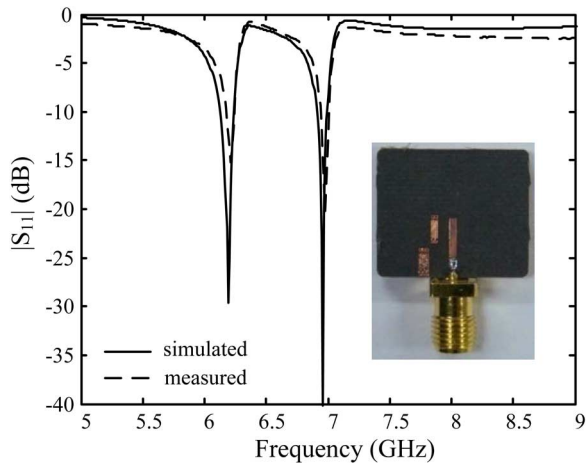

Fig. 15. Photograph and S_{11} reflection coefficient values of the dual-band MZR antenna.

that some radiated power is due to ground resonance. In any case, the radiation is dominated by the MZR antenna.

Fig. 12(a) shows a photograph of a three-cell MZR antenna using an IDC with four fingers as an example. The dimensions of the feed line for impedance matching are given by the method described in Section III-B, as shown in Fig. 12(a). Fig. 12(b) shows the simulated and measured results of the antenna including the SMA connector. The measured results are in good agreement with the simulated results. The -10 dB fractional bandwidths were simulated and measured as 3.8% and 4.9%, respectively. These values are different due to the rather poor matching from the fabrication tolerance, as shown in Fig. 12(b).

Fig. 13 shows the measured and simulated co-polarization and cross-polarization radiation patterns of the three-cell MZR antenna. According to coordination in Fig. 9, the co-polarization in the x-z plane and in the y-z plane corresponds to the radiated electric field in the ϕ-direction and in the θ-direction, respectively. In Fig. 13, the difference between the co-and cross-polarizations is less than that of a conventional small-loop antenna because the current path in Fig. 9 tilts with respect to the y-axis. The measured maximum gain of the antenna was 3.9 dBi, whereas the simulated maximum gain of the antenna was 5.1 dBi. The simulated and measured maximum gains of cross-polarization are less than that of co-polarization by 12.5 dB and 11.7 dB, respectively. The gain difference between the

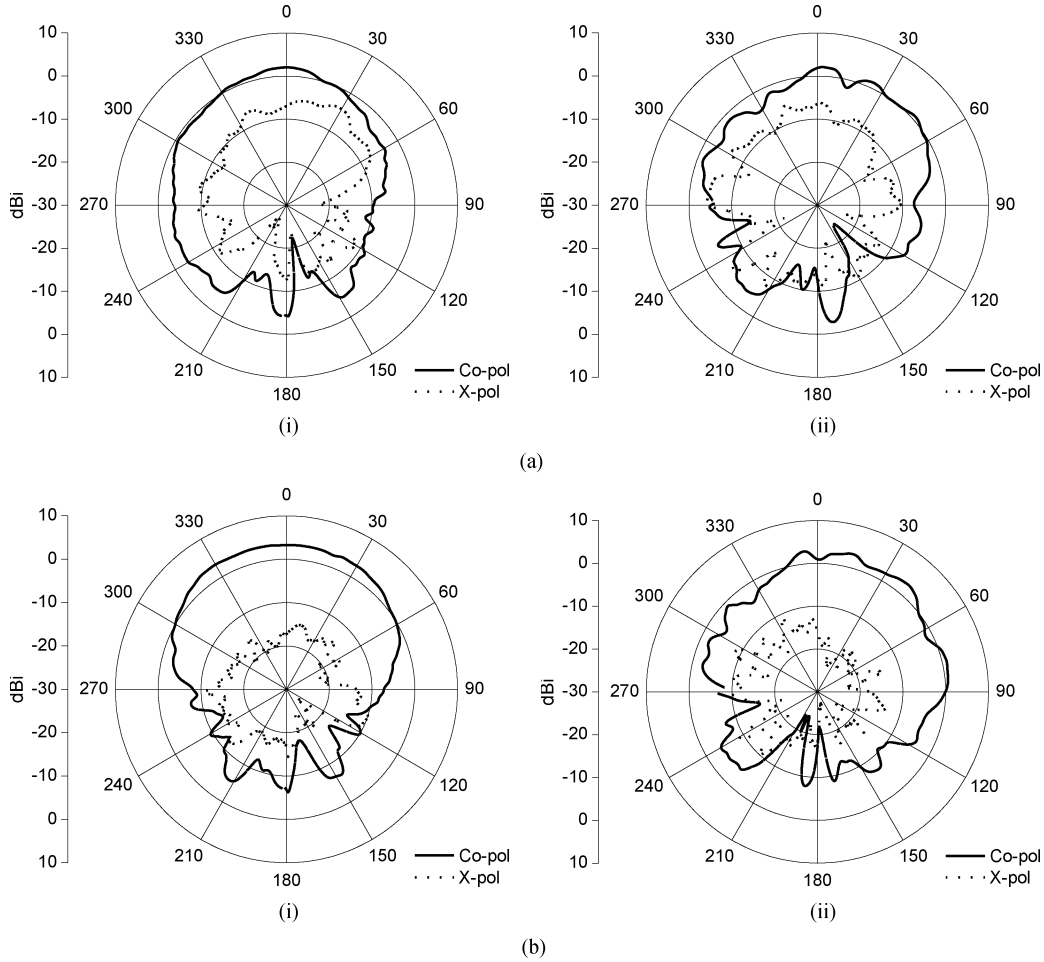

Fig. 16. Radiation patterns of the dual-band MZR antenna (a) First MZR frequency of 6.2 GHz (i) $\mathrm{Phi} = 0^\circ$ (x-z plane) (ii) $\mathrm{Phi} = 90^\circ$ (y-z plane) (b) Second MZR frequency of 7 GHz (i) $\mathrm{Phi} = 0^\circ$ (x-z plane) (ii) $\mathrm{Phi} = 90^\circ$ (y-z plane).

simulation and measurement of the MZR antenna is thought to be caused by mismatching from the dimensional tolerance of the fabrication and the smaller measured value of efficiency. It was also noted that the measured asymmetrical radiation pattern is due to the asymmetrical surface current, as mentioned earlier. The measured radiation patterns of MZR antennas have nulls and back-lobes due to the influence of the measuring cable. However, the measured results agree with the simulated results overall.

Finally, the fractional bandwidth and maximum gain of the antennas increase if the number of unit cells increases because the size of the in-phase current loop increases [21]. The radiation efficiencies were measured by the Wheeler cap method. To minimize the influence of the Wheeler cap on the current distribution on the MZR antenna, it is recommended that the cap radius of a spherical cap should be 1/6 λ [22]. However, our cap is not a sphere but a hexahedron. Thus, taking into account the hexahedral shape of the cap and the size of the MZR antenna, the size of the Wheeler cap was 40 mm in width, 32 mm in length, and 25 mm in height [23]. The TM_{110}, TM_{101}, and TM_{011} resonant modes of the cavity are 6 GHz, 7.07 GHz, and 7.61 GHz, respectively. For the one-cell MZR antenna with four fingers, the measured input impedances with and without the cap were 365-j5 and 74-j0.8 at 6.693 GHz and 6.635 GHz, respectively. Thus, the measured efficiency was determined to be 80% by calculating the above measured input impedance $((G_{\mathrm{no\_cap}} - G_{\mathrm{cap}})/G_{\mathrm{no\_cap}} = (365 - 74)/365)$. The measured efficiencies of the four MZR antennas in Table III are $76\% \sim 87\%$. The results show that the measured efficiencies are smaller than the simulated efficiencies, as shown in Table III. These smaller measured efficiencies may explain the smaller gains in the measurement shown in Table III. Consequently, the results of the size, bandwidth, efficiency, and gain show that the proposed MZR antenna can be successfully applied to antenna applications.

IV. Dual-Band MZR Antenna

The proposed MZR antennas are suitable for multiband applications because two or more MZR resonators with different resonant frequencies can easily be integrated using one feed line. Fig. 14 shows a dual-band MZR antenna using mu-zero resonators with four fingers and six fingers as an example. Here, the ground size is 20 mm $\times$ 17.5 mm. Two resonators are used: a one-cell resonator with six fingers and another with four fingers, corresponding to the MZR frequencies of 6.38 GHz and 7.03 GHz from (9) in Table III, respectively. For good impedance matching, the dimensions of the related feed line were chosen

to be $l_p = 8\,\mathrm{mm}$, $s_1 = 2.8\,\mathrm{mm}$, $s_2 = 1.6\,\mathrm{mm}$, $d_1 = 0.05\,\mathrm{mm}$, and $d_2 = 0.6\,\mathrm{mm}$, as discussed in Section III-B. The distance of s_2 is less than s_1, as shown in Fig. 14, because the magnetic coupling intensity is different as to the position of the radiator along the feed line. That is, the magnetic fields of the end of the feed line are weak because the feed line is open-ended. Therefore, the s_2 distance is smaller than the s_1 distance so as to obtain the required magnetic coupling.

Fig. 15 shows a photograph and the S_{11} reflection coefficient values of a dual-band MZR antenna. The simulated and measured reflection coefficient values show good agreement. The first and second MZR frequencies (and fractional $-10\,\mathrm{dB}$ bandwidths) are measured as frequencies of 6.2 GHz and 7 GHz (and 1.03% and 0.95%), respectively. The size of the antenna is $0.108\lambda_0 \times 0.175\lambda_0$ at the first MZR frequency and $0.121\lambda_0 \times 0.197\lambda_0$ at the second MZR frequency.

Fig. 16 shows the measured radiation patterns of the dual-band MZR antenna at the first and second MZR frequency. The two radiation patterns at two MZR frequencies have similar broadside patterns. The measured maximum gains of the antenna are as 2.3 dBi and 3.3 dBi at 6.2 GHz and 7 GHz, and the differences in the maximum gains between cross- and co-polarization are 6.5 dB and 11.2 dB, respectively. The patterns at 6.2 GHz have significantly higher cross-polarization components compared to those at 7 GHz for both the x-z and the y-z planes because the resonator at 6.2 GHz is close to the SMA connector. The efficiencies are 83% and 84% at 6.2 GHz and 7 GHz, respectively. Consequently, the proposed dual-band MZR antenna can easily be expanded by placing another MZR resonator beside the feed. It is also expected that the radiation characteristics at each band are similar.

V. Conclusions

A novel antenna using the mu-zero resonance of an artificial MNG metamaterial TL is presented. The equivalent circuit for verifying the peculiarity of the MNG TL is derived and analyzed. The feed lines for impedance matching and magnetic coupling are designed by circuit and full-wave simulation. The analysis and design of the MZR antenna were accomplished by theory and simulation based on a dispersion diagram and field distribution. The analyzed surface current has the characteristics of an in-phase loop current, indicating that the radiation mechanism of an MZR antenna is in essence identical to that of an electrical small-loop antenna. MZR antennas with one, two, and three unit cells were designed. Appling the novel concept of the MZR antenna, a dual-band MZR antenna using two MZR antennas with different MZR frequencies is presented. The measured characteristics show good agreement with the simulated values. The results also show that the dual-band MZR antenna can be expanded to a multiband antenna. Consequently, the proposed MZR antennas are suitable for antenna applications that require feasible gain, bandwidth, efficiency, and multiband characteristics. In particular, the size, gain, efficiency, and $-10\,\mathrm{dB}$ bandwidth of the dual-band MZR antenna are $0.108\lambda_0 \times 0.175\lambda_0$ ($0.121\lambda_0 \times 0.197\lambda_0$), 2.3 dBi (3.3 dBi), 83% (84%), and 1.03% (0.95%), at the first (second) MZR frequency, respectively.

References

[1] V. G. Veselago, "The electrodynamics of substances with simultaneously negative values of ε and μ," *Soviet Phys. Uspekhi*, vol. 10, no. 4, pp. 509–514, Jan. 1968.

[2] R. A. Shelby, D. R. Smith, and S. Schultz, "Experimental verification of a negative index of refraction," *Science*, vol. 292, pp. 77–79, Apr. 2001.

[3] N. Engheta and R. W. Ziolkowski, *Metamaterials: Physics and Engineering Explorations*. Hoboken, NJ: Wiley, 2006.

[4] C. Caloz and T. Itoh, *Electromagnetic Metamaterials: Transmission Line Theory and Microwave Applications*. Hoboken, NJ: Wiley, 2006.

[5] G. V. Eleftheriades and K. G. Balmain, *Negative-Refraction Metamaterials: Fundamental Principles and Applications*. Hoboken, NJ: Wiley, 2005.

[6] C. Caloz and T. Itoh, "Transmission line approach of left-handed (LH) materials and microstrip implementation of an artificial LH transmission line," *IEEE Trans. Antennas Propag.*, vol. 52, no. 5, pp. 1159–1166, May 2007.

[7] M. Gil, J. Bonache, J. Selga, J. Garcia-Garcia, and F. Martin, "Broadband resonant-type metamaterial transmission lines," *IEEE Microw. Wireless Compon. Lett.*, vol. 17, pp. 97–99, Feb. 2007.

[8] J. H. Park, Y. H. Ryu, J. G. Lee, and J. H. Lee, "A novel via-free composite right- and left-handed transmission line using defected ground structure," *IEEE Microw. Wireless Compon. Lett.*, vol. 49, no. 8, pp. 1989–1993, Aug. 2007.

[9] G. V. Eleftheriades, "Analysis of bandwidth and loss in negative-refractive-index transmission-line (NRI-TL) media using coupled resonators," *IEEE Microw. Wireless Compon. Lett.*, vol. 17, pp. 412–414, Jun. 2007.

[10] M. A. Antoniades and G. V. Eleftheriades, "A broadband series power divider using zero-degree metamaterial phase-shifting lines," *IEEE Microw. Wireless Compon. Lett.*, vol. 15, pp. 808–810, Nov. 2005.

[11] A. Sanada, C. Caloz, and T. Itoh, "Novel zeroth-order resonance in composite right/left- handed transmission line resonators," in *Proc. Asia-Pacific Microwave Conf.*, 2003, vol. 3, pp. 1588–1591.

[12] A. Sanada, M. Kimura, I. Awai, C. Caloz, and T. Itoh, "A planar zeroth-order resonator antenna using a left-handed transmission line," in *Proc. Eur. Microw. Conf.*, 2004, vol. 3, pp. 1341–1344.

[13] J. G. Lee and J. H. Lee, "Zeroth order resonance loop antenna," *IEEE Trans. Antennas Propag.*, vol. 55, no. 3, pp. 994–997, Mar. 2007.

[14] A. Rennings, T. Liebig, S. Abielmona, C. Caloz, and P. Waldow, "Tri-band and dual-polarized antenna based on composite right/left-handed transmission line," in *Proc. Eur. Microw. Conf.*, Oct. 2007, pp. 720–723.

[15] A. Rennings, T. Liebig, C. Caloz, and P. Waldow, "MIM CRLH series mode zeroth order resonant antenna (ZORA) implemented in LTCC technology," in *Proc. Asia-Pacific Microw. Conf.*, Dec. 2007, pp. 1–4.

[16] M. A. Antoniades and G. V. Eleftheriades, "A folded-monopole model for electrically small NRI-TL metamaterial antennas," *IEEE Antennas Wireless Propag. Lett.*, vol. 7, pp. 425–428, 2008.

[17] R. W. Ziolkowski, "An efficient, electrically small antenna designed for VHF and UHF applications," *IEEE Antennas Wireless Propag. Lett.*, vol. 7, pp. 217–220, 2008.

[18] A. Lai, K. M. K. H. Leong, and T. Itoh, "Infinite wavelength resonant antennas with monopolar radiation pattern based on periodic structures," *IEEE Trans. Antennas Propag.*, vol. 55, no. 3, pp. 868–876, Mar. 2007.

[19] J. H. Park, Y. H. Ryu, J. G. Lee, and J. H. Lee, "Epsilon negative zeroth-order resonator antenna," *IEEE Trans. Antennas Propag.*, vol. 55, no. 12, pp. 3710–3712, Dec. 2007.

[20] J. J. Carr, *Practical Antenna Handbook*. : McGraw-Hill, Press, 2001.

[21] L. J. Chu, "Physical limitations on omni-directional antennas," *J. Appl. Phys.*, vol. 19, pp. 1163–1175, Dec. 1948.

[22] D. M. Pozar and B. Kaufaman, "Comparison of three methods for the measurement of printed antenna efficiency," *IEEE Trans. Antennas Propag.*, vol. 36, pp. 136–139, Jan. 1988.

[23] H. Choo, R. Rogers, and H. Ling, "On the Wheeler cap measurement of the efficiency of microstrip antennas," *IEEE Trans. Antennas Propag.*, vol. 53, no. 7, pp. 2328–2332, Jul. 2005.

Jae-Hyun Park received the B.S. degree in electronic and electrical engineering and the M.S. degree in electronic information and communication engineering from Hongik University, Seoul, Korea, in 2005 and 2008, respectively, where he is currently working toward the Ph.D. degree.

His research interests include metamaterial RF devices and wireless power transfer systems.

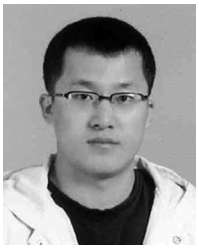

Young-Ho Ryu received the B.S. degree in electronic and electrical engineering from Jeju National University, Seoul, Korea, in 2003 and the M.S. and Ph.D. degrees in electrical engineering and computer science from Kyungpook National University, Daegu, Korea, in 2005 and 2009, respectively.

He is currently an R&D staff member at Samsung Advanced Institute of Technology. His research interests include metamaterial RF devices and wireless power transfer systems.

Jeong-Hae Lee (M'XX) received the B.S. and M.S. degrees in electrical engineering from Seoul National University, Korea, in 1985 and 1988, respectively, and the Ph.D. degree in electrical engineering from the University of California, Los Angeles, in 1996.

From 1993 to 1996, he was a Visiting Scientist of General Atomics, San Diego, CA, where his major research was to develop the millimeter wave diagnostic system and to study the plasma wave propagation. Since 1996, he has been at Hongik University, Seoul, Korea, where he is a Professor of Department of Electronic and Electrical Engineering. His current research interests include the microwave/millimeter wave circuits, the millimeter wave diagnostic, and the metamaterial RF devices.